International Journal of Biological Macromolecules 143 (2020) 825–832

Contents lists available at ScienceDirect

International Journal of Biological Macromolecules

journal homepage: http://www.elsevier.com/locate/ijbiomac

Chitosan-pluronic based Cu nanocomposite hydrogels for prototype antimicrobial applications

Tippabattini Jayaramudu [a,*], Kokkarachedu Varaprasad [b], K. Koteshwara Reddy [a], Radha D. Pyarasani [c], A. Akbari-Fakhrabadi [d], John Amalraj [a,*]

[a] Laboratory of Materials Science, Instituto de Química de Recursos Naturales, Universidad de Talca, 747, Talca, Chile
[b] Centre de Investigaciòn de Polìmeros Avanzados (CIPA), Avenida Collao 1202, Edificio de Laboratorios, Concepciòn, Chile
[c] Vicerrectoria de Investigaciòn y Postgrado, Universidad Católica del Maule, Talca, Chile
[d] Advanced Materials Laboratory, Department of Mechanical Engineering, University of Chile, Beauchef 851, Santiago, Chile

ARTICLE INFO

Article history:
Received 21 August 2019
Received in revised form 22 September 2019
Accepted 26 September 2019
Available online 9 November 2019

Keywords:
Chitosan
Copper nanoparticles
Nanocomposite hydrogels

ABSTRACT

Copper nanoparticles were synthesized via precipitation technique using the pseudonatural cationic chitosan biopolymer as a stabilizing agent. The nanoparticles developed were successfully incorporated into the 1:1 ratio of blended chitosan: pluronic F127 polymer solution and made their nanocomposite hydrogels by solution casting method. The formed copper-based nanocomposite hydrogels were characterized by using Fourier transform infrared spectroscopy, thermogravimetric analysis, X-ray diffraction, scanning electron microscopy-energy dispersive spectroscopy and transmission electron microscopy studies. The antimicrobial activity of the fabricated nanocomposite hydrogels was tested via an inhibition zone process against both *E. coli* (gram-negative) and *S. aureus* (gram-positive) bacteria. The results conveyed that the copper-embedded chitosan-pluronic\ F127 nanocomposite hydrogels can be used effectively for antimicrobial applications as well as for wound care applications.

1. Introduction

Currently, the applications of metal nanoparticles (NPs) and their nanocomposite materials have been majorly reported depending on their structural and surface characteristics [1,2]. Typically, NPs with an average one-dimensional size of ≤100 nm have been examined towards various applications such as biological, pharmaceutical, chemical manufacturing, catalysis, environmental technology and energy storage and conversion [2–6]. The great interest in the field of wound care/antimicrobial using NPs has incited the synthesis and investigation of NPs with distinctive nanostructures [7,8]. Inhibition of bacterial growth is one of the most noteworthy properties in wound care/antimicrobial application. The study of inhibition has been facilitated by rapid development in synthetic methodology. It has been aided by the synthesis of NPs with tunable properties such as shape, size and nanostructures either on their own or supported with other materials [9,10]. A variety of NPs and composite materials have been reported with excellent antimicrobial activity specifically copper, silver, gold, zinc oxide, platinum NPs, etc., [10–13]. Among the existing nanomaterials, copper nanoparticles (Cu NPs) have been selected for investigating the antimicrobial applications because it has been reported that Cu NPs possess superior antimicrobial activity compared to the other metal NPs [14,15].

Copper (Cu) is naturally abundant and inexpensive which offer the facile fabrication of multiple materials. Cu is a 3d transition metal which possesses impressive physicochemical characteristics. Cu-based nanocomposite materials have been attracted considerable interest due to their potential applications in various industrial and technological fields [16,17]. However, the use of Cu NPs is restricted by their own inherent instability under environmental and various reaction conditions, which makes it prone to oxidation. Due to these properties, the synthesized Cu NPs consisted of different oxidation states that are: Cu^0, Cu^I, Cu^{II} and Cu^{III} [18]. Owing to these oxidation states, many research groups have focused on the synthesis of Cu-based materials for various applications. Moreover, Nanoscience and nanotechnology enhance the utilization of the Cu-based nanomaterials for biomedical/wound care applications [19,20]. In view of nanotechnology, the Cu NPs can be prepared by several methods, such as metal vapor synthesis, sonochemical reduction, thermal reduction and chemical reduction [21–26]. Among the techniques, chemical reduction is the most popular technique that offers very good control of their nanostructural characteristics like shape and size. Recently, size-tunable Cu and copper oxide nanoparticles have been developed via reverse microemulsion using hydrazine hydrate and sodium borohydride as reducing agents [27]. However, these materials are not suitable for biomedical

* Corresponding authors.
E-mail addresses: jtibbabattini@utalca.cl, mr.jayaramudu@gmail.com (T. Jayaramudu), jamalraj@utalca.cl (J. Amalraj).

https://doi.org/10.1016/j.ijbiomac.2019.09.143
0141-8130/

applications due to the use of toxic solvents and hazardous chemicals as a reducing agent. To overcome this problem, researchers have introduced the green chemical process. In the green chemical process eco-friendly, safe and non-toxic chemicals are used [11,28]. Therefore, the development of Cu NPs based on the green chemical process is considered as the most appropriate method for wound care applications. Furthermore, Ancient Egyptians used copper vessels for purification of water and according to scientists, it has been known that copper can destroy a wide range of microorganisms such as *E. coli* and *S. aureus* naturally. These two are the most commonly found bacteria in the environment and are the general source of infection.

Herein, Cu NPs were developed by a facile chemical synthesis process using ascorbic acid as a reducing agent. The NPs were developed in the presence of chitosan (CH) which could act as a stabilizing agent and control the agglomeration of nanoparticles during the formation. The agglomeration was controlled through a coordination bond between the Cu NPs and amino and hydroxyl functional groups of CH polymer [29]. The synthesized CHCu NPs were successfully incorporated into a 1:1 ratio of CH:PF 127 (pluronic F127) blended solution to fabricate the nanocomposite hydrogels (CPF-CHCu) via solution casting technique. Crystallinity, surface morphology and particle size of the developed materials were studied using the x-ray diffraction, scanning electron microscopy and transmission electron microscopy. The inhibition of bacteria was tested against *E. coli* and *S. aureus* bacteria by using a standard disc method.

2. Materials and methods

2.1. Materials

Chitosan (CH) medium molecular weight with a Brookfield viscosity of 200–800 cP (CAS Number 9012-76-4) and Pluronic F 127 (PF 127) (CAS Number 9003-11-06) were purchased from Sigma Aldrich chemicals (Chile, South America). Sodium hydroxide, acetic acid, L-ascorbic acid, copper sulphate pentahydrate ($CuSO_4 \cdot 5H_2O$) and glutaraldehyde were purchased from Merck chemicals (Chile, South America). All the chemicals were used without further purification and double distilled water was used throughout the experiment.

2.2. Synthesis of CHCu-based CPF nanocomposite hydrogels

2.2.1. CHCu NPs

Accurately 0.1 g of CH was weighed and dissolved in 20 mL of double distilled water containing 0.3 mL of acetic acid in a 250 mL round bottom flask and heated to 85 °C. To this solution, 80 mL of an aqueous

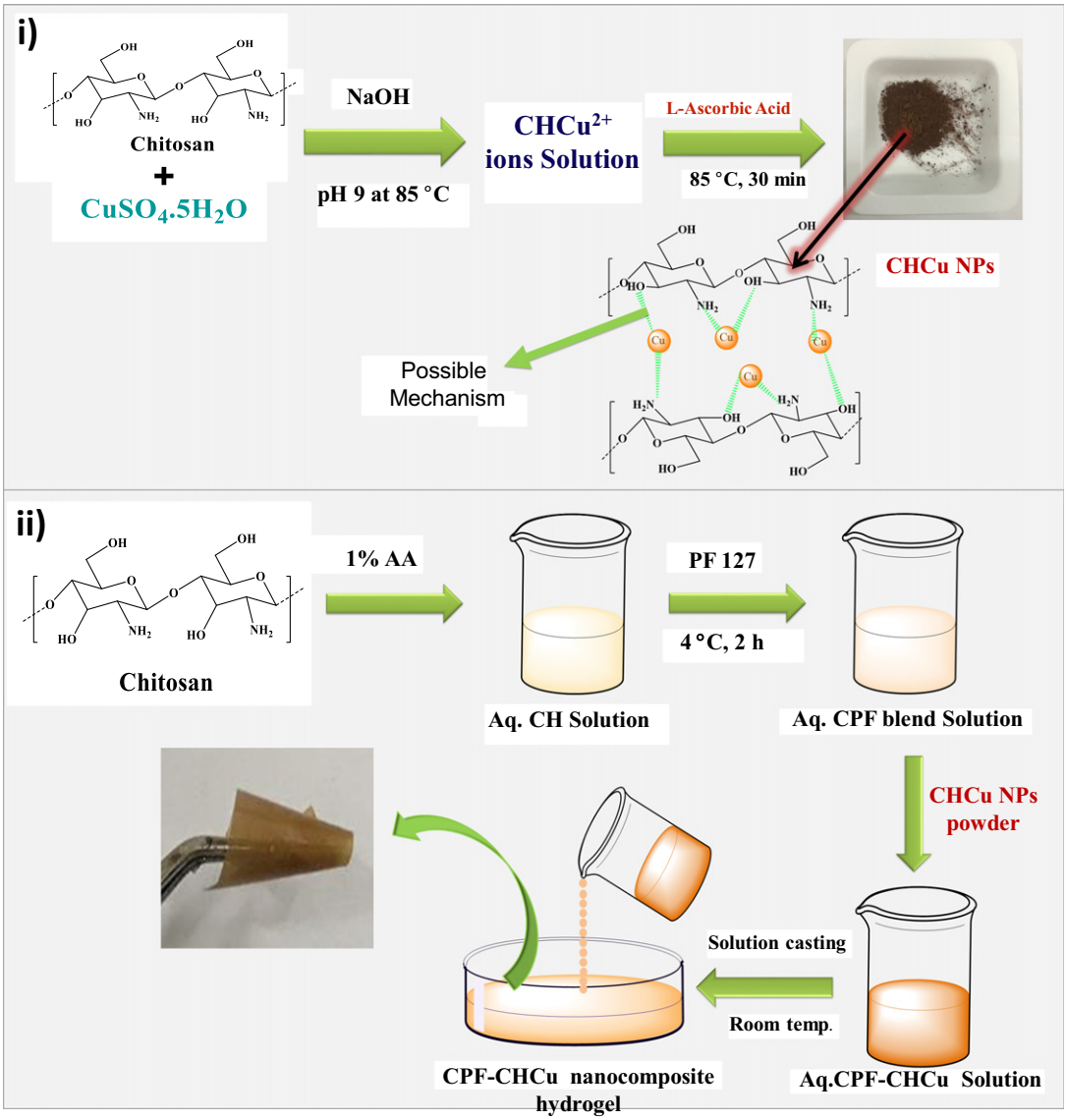

Fig. 1. Formation of A) CHCu NPs and B) CPF-CHCu nanocomposite hydrogels.

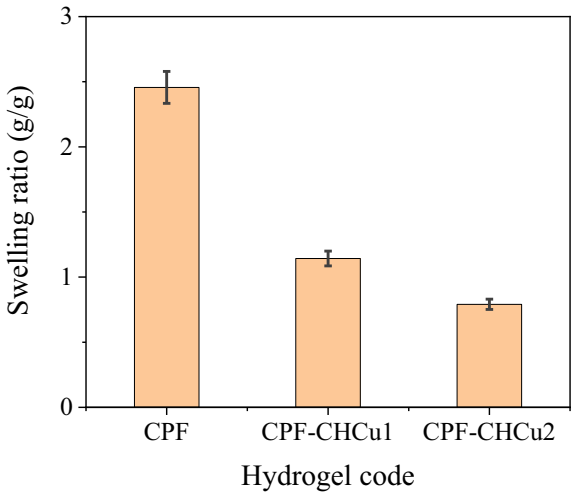

Fig. 2. Swelling ratio studies.

solution containing 2.5 g of copper sulphate pentahydrate was added slowly under constant stirring on a magnetic stirrer with 300 rpm over a period of 30 min. Then, pH of the reaction mixture was adjusted to ~ 9 by drop by drop addition of 0.5 M sodium hydroxide. During this moment, the solution colour was changed from light blue to dark blue and the reaction was further continued for another 30 min for successful completion of reaction which led to the dark blue colour of the entire solution. Then, a certain amount of ascorbic acid (0.625 M) solution was added in a dropwise manner and the stirring was continued for another 30 min. Immediately, the solution turned to yellow and then changed to red at the completion of the reaction. The red colour of the reaction mixture indicates the successful and complete formation of Cu NPs. Fig. 1A explains the schematic formation of the proposed CHCu NPs. The formed material was cooled and washed repeatedly with double distilled water through centrifugation at 8000 rpm. Finally, the obtained material was dried in a vacuum oven and stored in vacuum desiccator until used.

2.2.2. CPF-CHCu nanocomposite hydrogels

Prior to developing CPF-CHCu nanocomposite hydrogels, 1 g of CH was dissolved in 1% v/v aqueous acetic acid in a 250 mL round bottom flask at 60 °C for 6 h. After that, the temperature was brought down to ambient temperature. Then, the round bottom flask was kept in ice-cold water under constant stirring. Then, 1 g of PF127 was added to the above solution with constant stirring for another 2 h in order to get homogeneous CPF blended solution. The Obtained blended solution was divided into two parts and were taken in 100 mL round bottom flask. In one part 20 mg and in another part 40 mg of CHCu NPs powder was added and continued stirring to get a homogeneous mixture. The achieved homogeneous solution was poured into a petri dish and allowed to dry at ambient temperature. The formed hydrogels were peeled off from the petri dish and dried in a vacuum oven at 60 °C. The fabricated hydrogels were labelled as CPF-CHCu1 (20 mg of CHCu NPs) and CPF-CHCu2 (40 mg of CHCu NPs) nanocomposite hydrogels, respectively. Fig. 1B shows the schematic preparation of the nanocomposite hydrogel. In the similar way the CPF hydrogel was prepared following the above procedure with 1:1 ratio of CH (0.5 g): PF 127 (0.5 g) without CHCu NPs.

2.3. Characterizations

Attenuated total reflection-Fourier transform infrared (ATR-FTIR) (UATR two, Beaconsfield, Bucks, UK) spectrometer was used to analyze the formation of CHCu NPs, CPF and their nanocomposite hydrogels. FTIR spectra of the samples were recorded in a range from 400 to 4000 cm^{-1} with 16 average scans on the ATR-FTIR. The crystalline structure of the synthesized materials was characterized by using the X-ray diffraction technique (XRD, Bruker D8 using TOPAS 4.2 software) with Cu Kα radiation source (λ = 50.1546 nm) at 15 kV and 50 mA. The scan speed was 2 degree per min and the spectra of 2θ (Bragg angle) range was 5°-80°. Differential scanning calorimetry (DSC) thermograms of the prepared materials were recorded using a DSC 882e, Mettler Toledo instrument at a heating rate of 5 °C /min under constant nitrogen flow (100 mL/min) in the temperature range of 25–300 °C. Thermal stability of the samples were studied with a thermogravimetric analyser (TGA) (TGA Q50 thermal analyser, TA Instruments–Waters, LLC, Newcastle, DE) in the temperature range of 25–600 °C with a heating rate of 10 °C/min under constant nitrogen flow (100 mL/min).

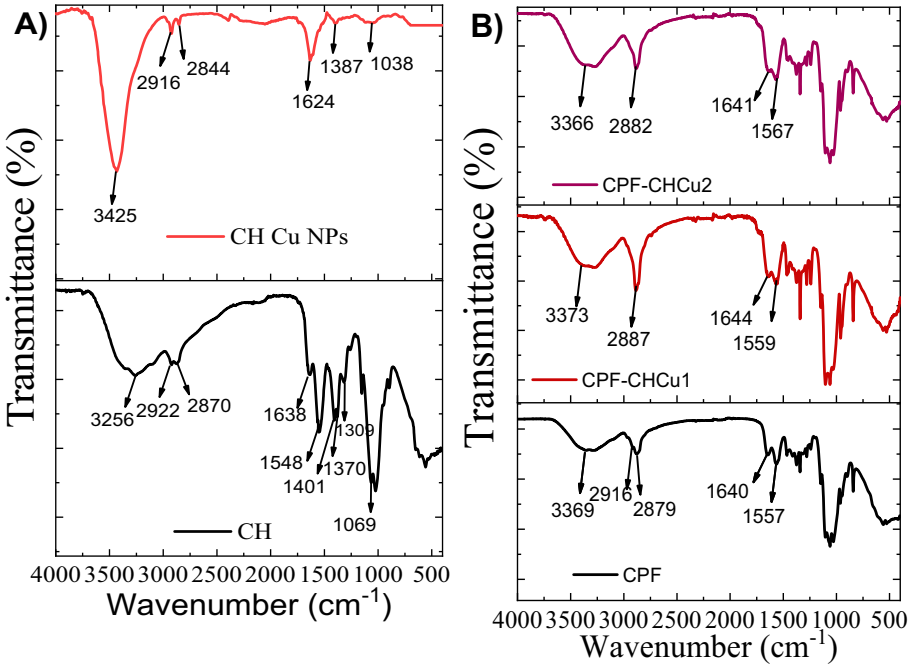

Fig. 3. FTIR spectra of (A) CH, and CHCu NPs, (B) CPF, CPF-CHCu1 and CPF-CHCu2 nanocomposite hydrogels.

The surface morphology of the samples was observed by using Scanning electron microscopy (SEM) using a JEOL JEM-7500F instrument (Tokyo, Japan). The samples were gold coated before the SEM analysis and were scanned at an accelerating voltage of 10 kV. Nanostructural morphology of the synthesized NPs was studied from transmission electron microscopy (TEM) (Tecnai G^2 F20FEG and FEI TITAN G2 880-300) analysis. The NPs were dispersed in the double distilled water (1 mg/1 mL). Two to three drops of the sample were deposited on a holey carbon Cu 300 mesh, 50-μm (HC300-CU) TEM grid with the help of a 10 μL micro pipette and dried on a filter paper at ambient temperature.

2.4. Antimicrobial activity studies

Antimicrobial activity of the prepared materials was studied via inhibition zone method using *E. coli and S. aureus* bacteria as a gram-negative and gram-positive bacterium respectively. The test was conducted using a modified agar disc method for 48 h in the incubation chamber at 37 °C [30]. The nutrient agar medium was prepared by mixing the known amount of peptone (5.0 g), beef extract (3.0 g) and sodium chloride (5.0 g) in 1000 mL distilled water. pH was adjusted to 7.0 by using digital pH meter. Then, a known amount of agar (15.0 g) was added to the above solution. The agar medium was sterilized in a conical flask at a pressure of 6.8 kg (15 lbs) for 30 min. The sterilized medium was transferred into sterilized Petri dishes in a laminar airflow chamber and allow to solidify. After solidification, 50 μL of the bacteria culture (gram-positive bacteria, MTCC-7443 and gram-negative bacteria, MTCC-1668) was spread on the above solid surface [31]. Then, circular shape Whatman filter paper was dipped in CHCu (0.4 mg/mL and 0.8 mg/mL) NPs solutions. Similarly, nanocomposite hydrogels were cut into a circular shape with the help of punching machine and both materials were placed on the bacteria culture. Later, they were incubated for 48 h at 37 °C.

3. Results and discussion

3.1. Water uptake studies

The water uptake study plays a significant role in biomedical applications. The studies of the developed materials are shown in Fig. 2 which revealed that a number of water molecules absorbed and hold in their network structure [32]. For this, the certain weight (~40 ± 5 mg) of the prepared hydrogels were cut into a rectangular shape

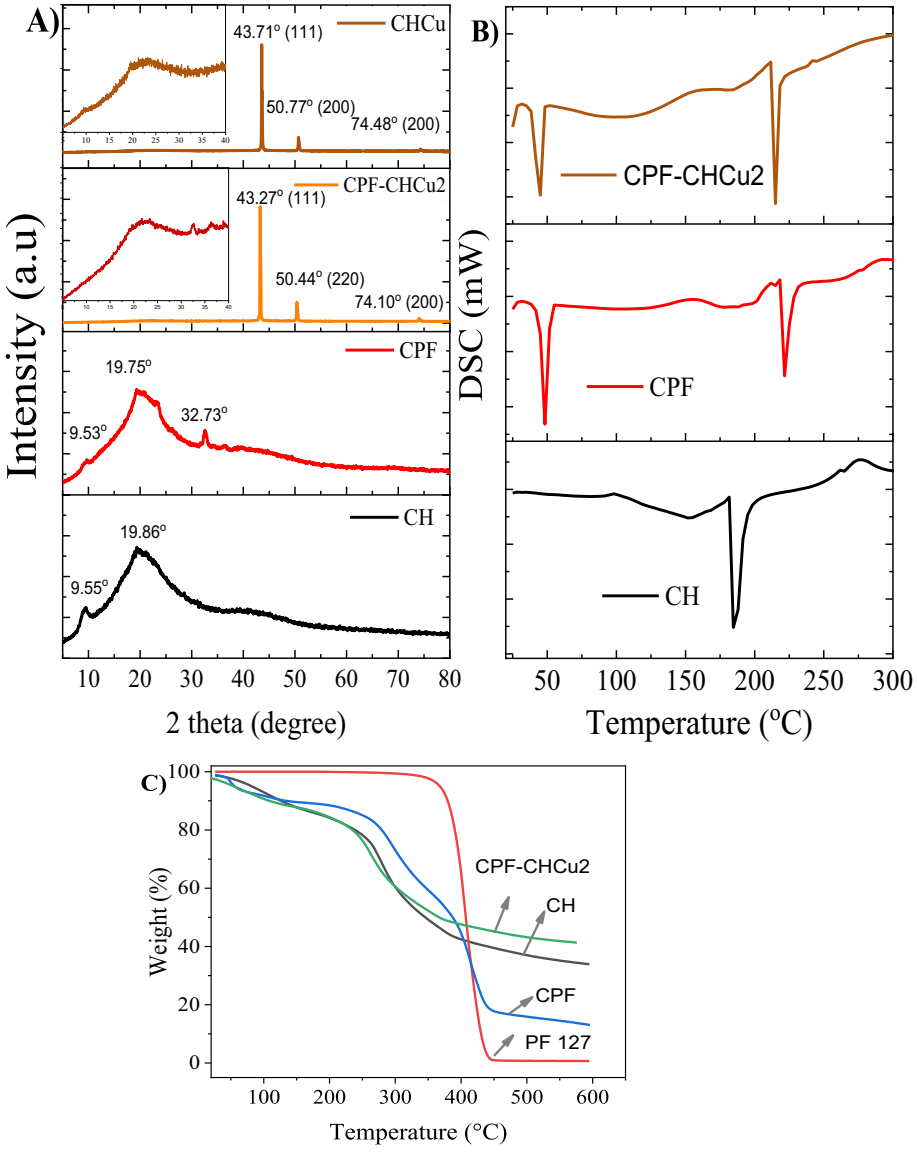

Fig. 4. (A) XRD spectra of CH, CPF, CPF-CHCu2 and CHCu NPs, (B) DSC of Pure CH, CPF and CPF-CHCu2 nanocomposite hydrogel and (C) TGA of Pure CH, PF127, CPF and CPF-CHCu2 nanocomposite hydrogel.

and dried in a vacuum oven for 6 h at 60 °C. Then, the dried hydrogels were immersed in a beaker containing 50 mL of double distilled water and allowed to swell for a period of 24 h. Weights of the hydrogels were noted before swelling (dry) and after swelling at equilibrium and the values are calculated using the below equation:

$$\text{Water uptake ratio } (S_{g/g}) = \frac{W_o - W_d}{W_d} \times 100 \quad (1)$$

Here, W_o and W_d denote the weight of the dry and swollen hydrogels. The experiment was carried out three times and average values were taken. From the Fig. 2, the pure CPF hydrogel absorbed 2.5 g/g of water molecules. Whereas, in the case of nanocomposite hydrogels, the water uptake capacity was completely depended on the used amount. For example, the CPF-CHCu1 exhibited the 1.2 g/g water uptake capacity and further it was decreased to 0.7 g/g (CPF-CHCu2). This behavior was observed due to the enhanced crosslinking network

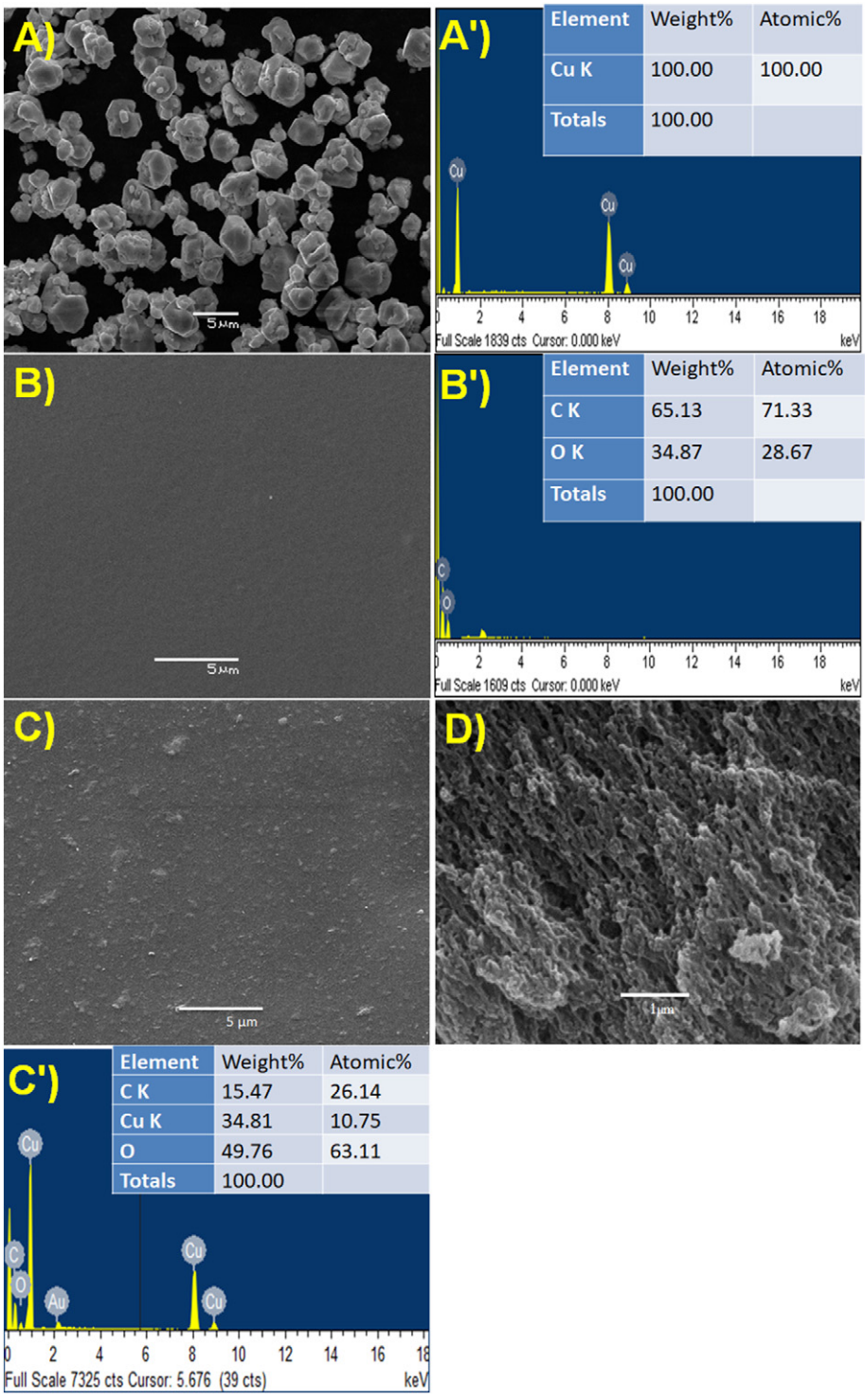

Fig. 5. SEM images of (A) CHCu NPs, (B) CPF-hydrogel, (C) CPF- CHCu2 nanocomposite hydrogel and (D) Cross-section image of CPF-CHCu2 nanocomposite hydrogel and EDS images: (A^I) CHCu NPs, (B^I) CPF-hydrogel and (C^I) CPF-CHCu2 nanocomposite hydrogel.

between the CPF blended solution and CHCu NPs. Moreover, this behavior also depends on the filler concentration and porosity [32].

3.2. ATR-FTIR analysis

The FTIR spectroscopy is an effective and easy way to identify the functional groups of the synthesized material. Structural analysis of the prepared materials was performed by comparing the ATR-FTIR spectra of CPF-CHCu2 with those of CH, CHCu and CPF (Fig. 3). From the Fig. 3A, the pure CH displayed a broad characteristic peak at 3256 cm^{-1}, corresponding to the —OH and —NH stretching vibrations and the peaks at 2922 and 2870 cm^{-1} were relevant to the —CH symmetric and asymmetric stretching vibrations and the peaks at 1638 and 1548 cm^{-1} indicated the —NH_2 bending vibrations. The —CH bending vibrations were observed at 1401, 1370 and 1309 cm^{-1}. The peak at 1069 cm^{-1} specified the skeletal frequency of —C—O—C— [24]. The CHCu NPs exhibited a shift and change in the CH characteristic peaks, especially the —OH and —NH stretching vibrations appeared at 3425 cm^{-1}. The observed shifting was majorly due to the formation and stabilization of Cu NPs. Fig. 3B shows the FTIR spectra of the CPF and CHCu NPs based CPF-CHCu nanocomposite hydrogels. The CPF hydrogel showed the similar peaks of the CH but the peak positions were changed because of the blending of PF127. For example, the peak at 3369 cm^{-1} was associated with the —OH and —NH stretching vibration, 2916 and 2879 cm^{-1} peaks corresponding to the —CH symmetric and asymmetric vibrations. Peaks at 1640 and 1557 cm^{-1} correspond to —NH bending vibrations. Even after the formation of CHCu NPs based nanocomposite hydrogels displayed similar characteristic peaks of the CPF with a minor change in their wavenumber. The upshifting of the peak in wavenumber was observed with the increasing of CHCu NPs. It can be concluded that the coordination bonds have been formed in the resultant CPF-CHCu nanocomposite hydrogels.

3.3. X-ray diffraction analysis

XRD analysis explains the crystallinity of materials as crystalline, semi-crystalline and amorphous. XRD patterns of the pure CH, CPF, CHCu and CPF-CHCu2 nanocomposite hydrogels were represented in Fig. 4A. CH is known to be a semi-crystalline polysaccharide material. Due to this nature, the pure CH displays two well-defined diffraction peaks at $2\theta = 9.55$ and 19.86° in their XRD patterns [33,34]. The CHCu NPs showed three diffraction peaks at $2\theta = 43.71$, 50.77 and 74.48° corresponding to the crystalline planes of the face-centered cubic structure of copper and it was consistent with the data of JCPDS No. 85-1326. The inset picture clearly showed the CH peaks, were well capped with Cu NPs, which was confirmed from the FTIR spectra as well (Fig. 3A). The CPF hydrogel showed similar peaks of CH shown at $2\theta = 9.53$ and 19.75° apart from this a new peak was observed at $2\theta = 23.54$ and 32.73° corresponding to the PF127 [35,36]. In the case of CPF-CHCu2 nanocomposite hydrogels showed all the above CPF (inset figure) peaks with additional diffraction peaks at $2\theta = 43.27$ (1 1 1), 50.44 (2 0 0) and 74.10° (2 2 0) corresponding to the Cu NPs.

3.4. DSC-TGA analysis

DSC is a useful and well-established technique that can determine the glass transition temperature of the blended composition. DSC thermograms of the pure CH, CPF and CPF-CHCu nanocomposite hydrogels were represented in Fig. 4B. The thermogram of chitosan shows two endothermic peaks at 152.3 and 184.89 °C related to the crystallization temperature and melting temperature of the CH. The CPF showed comparable endothermic peaks with changing the temperatures at 186 and 222.1 °C and a new sharp endothermic peak was appeared at 48.71 °C. The CH endothermic peak shifted to higher temperature due to the blending of PF127 to CH. On the other hand, CPF-CHCu nanocomposites exhibited peaks at 44.81, 184 and 215.56 °C. The DSC peaks of CPF shifted to a lower temperature in CPF-CHCu nanocomposite conveying that the CPF (chitosan and PF127) chains of complexes can be broken more easily in the presences of Cu NPs than the pure materials.

Thermal properties such as stability and decompositions were studied by using TGA analysis as a function of temperature *vs* weight loss. Fig. 4C shows TGA curves of CH, PF127, CPF and CPF-CHCu nanocomposite hydrogels under constant nitrogen flow. Except for PF127, 10% initial weight loss was observed in the temperate range between 58 and 130 °C. It was due to the evaporation of physically adsorbed water. The actual thermal degradation was noticed in the range of 210–382 °C for pure CH, 350–445 °C for PF 127 and 255–435 °C for the CPF hydrogel. When compared to PF127, the CPF hydrogel showed lower degradation temperature, possibly due to the formation of crosslinking between the CH and PF 127. The CPF-CHCu nanocomposite hydrogel showed faster degradation (212–365 °C) than that of CPF hydrogel. This behavior could be majorly attributed to the surface interaction of Cu nanoparticles and CPF which enhanced the heat transfer between the Cu NPs and CPF polymer chains, respectively. Wael et al. observed a similar trend in the case of solid-state silver and gold metal nanoparticles supported by cellulose nanocrystals and developed hybrid materials have been used for catalytic applications [37]. At the end of the thermal degradation (550 °C), the component material was burned off and the leftover material was 35.3% (CH), 0.8% (PF127), 14.5% (CPF) and 42.1% (CPF-CHCu nanocomposite), respectively.

3.5. SEM and TEM analysis

Nanostructural morphologies of the synthesized materials were studied using scanning electron microscopy. SEM images of the CHCu

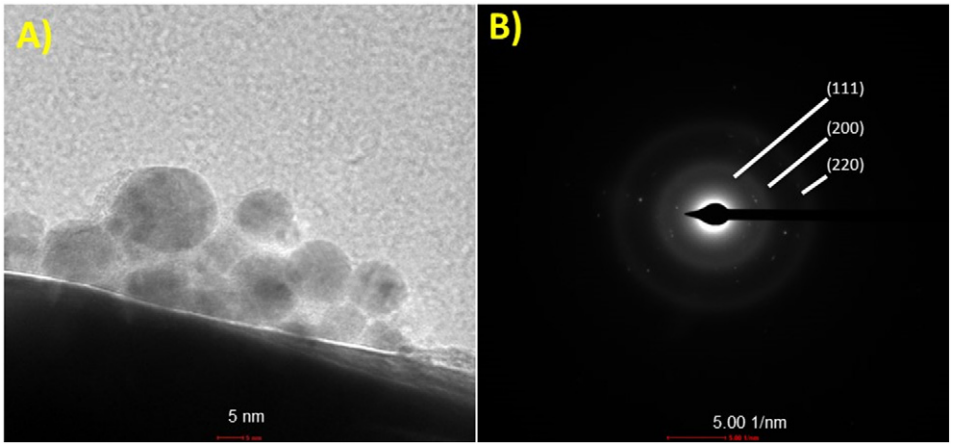

Fig. 6. TEM images of (A) CHCu NPs and (B) SAED pattern of CHCu NPs.

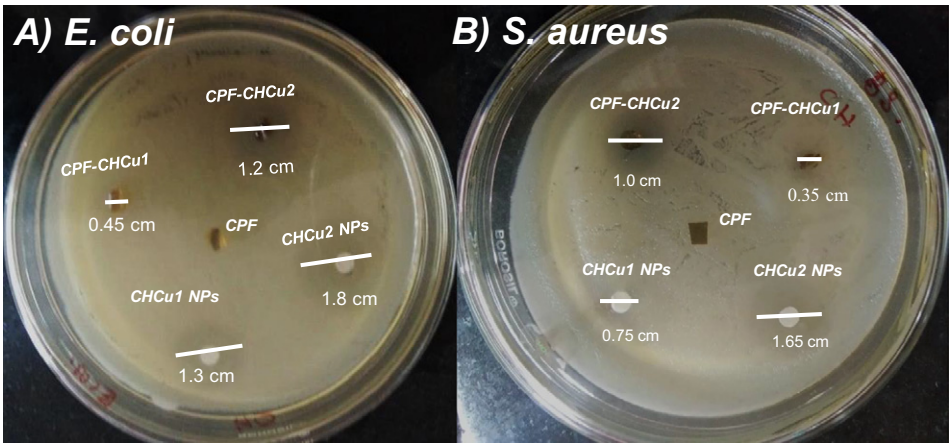

Fig. 7. Antimicrobial activity of the developed materials against (A) *E. coli* and (B) *S. aureus*.

NPs, CPF and CPF-CHCu2 nanocomposites hydrogels were depicted in Fig. 5. The CHCu NPs showed a spherical structure (Fig. 5A). Whereas the CPF hydrogels showed smooth surface area (Fig. 5B). The CHCu NPs dispersed (CPF-CHCu2) nanocomposite hydrogels showed rough surface morphology (Fig. 5C). Fig. 5D showed the cross-section image of the CPF-CHCu2 nanocomposite hydrogels. Elemental analysis of all the samples was shown in Fig. 5. A^{l}-C^{l} and it was studied using the energy dispersive spectroscopy (EDS). The EDS spectra showed clear peaks of the Cu NPs. Overall the SEM/EDS analysis demonstrates that the PF 127 and CHCu NPs were well dispersed in the CH and CPF to form their corresponding nanocomposite hydrogels, respectively.

Fig. 6 shows the nanostructure morphology of the developed CHCu NPs, which was studied by using the TEM. From the Fig. 6A the CHCu NPs were observed in uniform spherical structure with an average diameter of ~8 ± 2 nm and Fig. 6B shows the selected area electron diffraction pattern of the synthesized CHCu NPs.

3.6. Antimicrobial activity

The antimicrobial activity of the developed materials (CHCu NPs, CPF, CPF-CHCu1 and CPF-CHCu2) was studied against gram-negative (*E. coli*) and gram-positive (*S. aureus*) bacteria using disc method. The efficiency of antimicrobial activity was measured via an inhibition zone after 48 h incubation at 37 °C. The antimicrobial activity of CHCu NPs, CPF, CPF-CHCu1 and CPF-CHCu2 nanocomposite hydrogels are shown in Fig. 7. The results indicated that the synthesized CHCu NPs and their nanocomposite hydrogels exhibited significant antimicrobial activity against both *E. coli* and *S. aureus* bacteria, whereas CPF hydrogel did not show any antimicrobial activity. In contrast, a significant antimicrobial activity was observed for the CPF-CHCu2 (*E. coli* = 1.2 cm and *S. aureus* = 1.0 cm) and CHCu NPs (0.8 mg/mL) (for *E. coli* = 1.8 cm and *S. aureus* = 1.65 cm) had the strongest antimicrobial activity when compared to the CPF-CHCu1 (*E. coli* = 0.45 cm and *S. aureus* = 0.35 cm) and CHCu NPs (0.4 mg/mL) (*E. coli* = 1.3 cm and *S. aureus* = 0.75 cm), respectively. Overall, the antimicrobial activity of the CHCu NPs, CPF-CHCu1 and CPF-CHCu2 nanocomposite hydrogels is mainly attributed to the release of Cu NPs. The released Cu NPs inhibit the bacterial growth in two pathways: (1) depolarization of the cell's membrane through interaction between the cell's membrane and Cu NPs which caused weakening the cell's outer membrane. (2) Cu^{2+} ions initiated after the oxidation of Cu NPs, which are penetrated into the cell's and mediated the reactive oxygen species, caused blocking the bacterial cell's metabolism resulting in cell death. These results revealed that the developed materials possessed the strong antimicrobial activity on both gram-positive and gram-negative bacteria. However, the synthesized materials were exhibited highest antimicrobial activities against *E. coli* than the *S. aureus*. This behavior mainly due to the electrostatic interaction between the negatively charged bacterial cell membrane of the *E. coli* and the positively charged Cu NPs [38]. Deryabin et al., investigated and reported the mechanism between the electrostatic interaction between *E. coli* and Cu nanoparticles [39]. As per the reported literature, the synthesized materials with the zone inhibition of >1.0 mm could be considered as a good antimicrobial agent [40,41].

4. Conclusion

In this report, we have synthesized chitosan stabilized copper nanoparticles (CHCu NPs) via a facile chemical reduction process using ascorbic acid as a reducing agent. The developed nanoparticles were successfully incorporated into a 1:1 ratio of blended chitosan-pluronic F127 (CPF) polymer solution and made their nanocomposite hydrogels by solution casting technique. The developed CHCu NPs and nanocomposite hydrogels were analysed by ATR-FTIR, XRD, DSC-TGA, SEM/EDS and TEM. The ATR-FTIR studies confirmed that the Cu NPs have stabilized with CH during the formation via coordination bond between the Cu NPs and CH Functional groups. The SEM and TEM studies revealed that the formed nanoparticles have a spherical structure with an average diameter of ~8 ± 2 nm. The efficiency of antimicrobial activity of the fabricated nanocomposite hydrogels was tested via disc method against both *E. coli* and *S. aureus*. The inhibition zone of bacteria depends on the amount of the Cu NPs. The inhibition zone area increased with the increasing amounts of the Cu NPs. The results conveyed that the Cu NPs incorporated chitosan-pluronic F127 nanocomposite (CPF-CHCu NPs) hydrogels can be used effectively in antimicrobial applications and wound dressing applications.

Acknowledgments

The author, Tippabattini Jayaramudu acknowledges the Fondecyt Postdoctoral Project No 3170272, which is supported by FONDECYT Postdoctoral Research and Universidad de Talca, 747, Talca, Chile. Authors acknowledge PIEI-QUIM-BIO, and Proyecto de Investigacion enlace FONDECYT (No 300061) Universidad de Talca. PR wishes to acknowledge VRIP, Universidad Catolica del Maule. KVP wishes to acknowledge Fondecyt 11160073 & CIPA, CONICYT Regional, GORE BIO-BIO, R17A10003.

References

[1] H.J. Kwon, K. Shin, M. Soh, H. Chang, J. Kim, J. Lee, G. Ko, B.H. Kim, D. Kim, T. Hyeon, Large-scale synthesis and medical applications of uniform-sized metal oxide nanoparticles, Adv. Mater. 30 (2018) 1704290, https://doi.org/10.1002/adma.201704290.
[2] Y. Zhou, C. Jin, Y. Li, W. Shen, Dynamic behavior of metal nanoparticles for catalysis, Nano Today 20 (2018) 101–120, https://doi.org/10.1016/j.nantod.2018.04.005.

[3] L. Chen, B. Su, L. Jiang, Recent advances in one-dimensional assembly of nanoparticles, Chem. Soc. Rev. 48 (2019) 8–21, https://doi.org/10.1039/C8CS00703A.
[4] S.M. Amini, Preparation of antimicrobial metallic nanoparticles with bioactive compounds, Mater. Sci. Eng. C 103 (2019) 109809, https://doi.org/10.1016/j.msec.2019.109809.
[5] C. Hu, L. Song, Z. Zhang, N. Chen, Z. Feng, L. Qu, Tailored graphene systems for unconventional applications in energy conversion and storage devices, Energy Environ. Sci. 8 (2015) 31–54, https://doi.org/10.1039/C4EE02594F.
[6] Y. Liu, Q. Zhang, M. Xu, H. Yuan, Y. Chen, J. Zhang, K. Luo, J. Zhang, B. You, Novel and efficient synthesis of Ag-ZnO nanoparticles for the sunlight-induced photocatalytic degradation, Appl. Surf. Sci. 476 (2019) 632–640, https://doi.org/10.1016/j.apsusc.2019.01.137.
[7] N. Krishnan, B. Velramar, B. Ramatchandirin, G.C. Abraham, N. Duraisamy, R. Pandiyan, R.K. Velu, Effect of biogenic silver nanocubes on matrix metalloproteinases 2 and 9 expressions in hyperglycemic skin injury and its impact in early wound healing in streptozotocin-induced diabetic mice, Mater. Sci. Eng. C 91 (2018) 146–152, https://doi.org/10.1016/j.msec.2018.05.020.
[8] G. Shi, W. Chen, Y. Zhang, X. Dai, X. Zhang, Z. Wu, An antifouling hydrogel containing silver nanoparticles for modulating the therapeutic immune response in chronic wound healing, Langmuir 35 (2019) 1837–1845, https://doi.org/10.1021/acs.langmuir.8b01834.
[9] T. Jayaramudu, G.M. Raghavendra, K. Varaprasad, G.V.S. Reddy, A.B.B. Reddy, K. Sudhakar, E.R. Sadiku, Preparation and characterization of poly(ethylene glycol) stabilized nano silver particles by a mechanochemical assisted ball mill process, J. Appl. Polym. Sci. 133 (2016) https://doi.org/10.1002/app.43027.
[10] G.M. Raghavendra, T. Jayaramudu, K. Varaprasad, R. Sadiku, S.S.S. Ray, K. Mohana Raju, Cellulose–polymer–Ag nanocomposite fibers for antibacterial fabrics/skin scaffolds, Carbohydr. Polym. 93 (2013) 553–560, https://doi.org/10.1016/j.carbpol.2012.12.035.
[11] T. Jayaramudu, K. Varaprasad, R.D. Pyarasani, K.K. Reddy, K.D. Kumar, A. Akbari-Fakhrabadi, R.V. Mangalaraja, J. Amalraj, Chitosan capped copper oxide/copper nanoparticles encapsulated microbial resistant nanocomposite films, Int. J. Biol. Macromol. 128 (2019) 499–508, https://doi.org/10.1016/j.ijbiomac.2019.01.145.
[12] K. Varaprasad, M. Pariguana, G.M. Raghavendra, T. Jayaramudu, E.R. Sadiku, Development of biodegradable metaloxide/polymer nanocomposite films based on poly-ε-caprolactone and terephthalic acid, Mater. Sci. Eng. C 70 (2017) 85–93, https://doi.org/10.1016/j.msec.2016.08.053.
[13] K.B. Ayaz Ahmed, T. Raman, V. Anbazhagan, Platinum nanoparticles inhibit bacteria proliferation and rescue zebrafish from bacterial infection, RSC Adv. 6 (2016) 44415–44424, https://doi.org/10.1039/C6RA03732A.
[14] E.J. Guidelli, A.P. Ramos, M.E.D. Zaniquelli, O. Baffa, Green synthesis of colloidal silver nanoparticles using natural rubber latex extracted from Hevea brasiliensis, Spectrochim Acta – Part A Mol. Biomol. Spectrosc. 82 (2011) 140–145, https://doi.org/10.1016/j.saa.2011.07.024.
[15] N. Cioffi, L. Torsi, N. Ditaranto, G. Tantillo, L. Ghibelli, L. Sabbatini, T. Bleve-Zacheo, M. D'Alessio, P.G. Zambonin, E. Traversa, Copper nanoparticle/polymer composites with antifungal and bacteriostatic properties, Chem. Mater. 17 (2005) 5255–5262, https://doi.org/10.1021/cm0505244.
[16] N. Verma, N. Kumar, Synthesis and biomedical applications of copper oxide nanoparticles: an expanding horizon, ACS Biomater. Sci. Eng. 5 (2019) 1170–1188, https://doi.org/10.1021/acsbiomaterials.8b01092.
[17] M. Rafique, A.J. Shaikh, R. Rasheed, M.B. Tahir, H.F. Bakhat, M.S. Rafique, F. Rabbani, A review on synthesis, characterization and applications of copper nanoparticles using green method, Nano 12 (2017) 1750043, https://doi.org/10.1142/S1793292017500436.
[18] M.B. Gawande, A. Goswami, F.-X. Felpin, T. Asefa, X. Huang, R. Silva, X. Zou, R. Zboril, R.S. Varma, Cu and Cu-based nanoparticles: synthesis and applications in catalysis, Chem. Rev. 116 (2016) 3722–3811, https://doi.org/10.1021/acs.chemrev.5b00482.
[19] T. Kruk, M. Gołda-Cępa, K. Szczepanowicz, L. Szyk-Warszyńska, M. Brzychczy-Włoch, A. Kotarba, P. Warszyński, Nanocomposite multifunctional polyelectrolyte thin films with copper nanoparticles as the antimicrobial coatings, Colloids Surf. B Biointerf. 181 (2019) 112–118, https://doi.org/10.1016/j.colsurfb.2019.05.014.
[20] G.M. Raghavendra, J. Jung, D. Kim, J. Seo, Chitosan-mediated synthesis of flowery-CuO, and its antibacterial and catalytic properties, Carbohydr. Polym. 172 (2017) 78–84, https://doi.org/10.1016/j.carbpol.2017.04.070.
[21] A.A. Ponce, K.J. Klabunde, Chemical and catalytic activity of copper nanoparticles prepared via metal vapor synthesis, J. Mol. Catal. A Chem. 225 (2005) 1–6, https://doi.org/10.1016/j.molcata.2004.08.019.
[22] N.A. Dhas, C.P. Raj, A. Gedanken, Synthesis, characterization, and properties of metallic copper nanoparticles, Chem. Mater. 10 (1998) 1446–1452, https://doi.org/10.1021/cm9708269.
[23] Q.B. Zhang, Y.X. Hua, Electrochemical synthesis of copper nanoparticles using cuprous oxide as a precursor in choline chloride–urea deep eutectic solvent: nucleation and growth mechanism, Phys. Chem. Chem. Phys. 16 (2014) 27088–27095, https://doi.org/10.1039/C4CP03041A.
[24] T. Abiraman, E. Ramanathan, G. Kavitha, R. Rengasamy, S. Balasubramanian, Synthesis of chitosan capped copper oxide nanoleaves using high intensity (30 kHz) ultrasound sonication and their application in antifouling coatings, Ultrason. Sonochem. 34 (2017) 781–791, https://doi.org/10.1016/j.ultsonch.2016.07.013.
[25] D. Mott, J. Galkowski, L. Wang, J. Luo, C.-J. Zhong, Synthesis of size-controlled and shaped copper nanoparticles, Langmuir 23 (2007) 5740–5745, https://doi.org/10.1021/la0635092.
[26] H. Ohde, F. Hunt, C.M. Wai, Synthesis of silver and copper nanoparticles in a water-in-supercritical-carbon dioxide microemulsion, Chem. Mater. 13 (2001) 4130–4135, https://doi.org/10.1021/cm010030g.
[27] A. Kumar, A. Saxena, A. De, R. Shankar, S. Mozumdar, Facile synthesis of size-tunable copper and copper oxide nanoparticles using reverse microemulsions, RSC Adv. 3 (2013) 5015, https://doi.org/10.1039/c3ra23455j.
[28] J. Suárez-Cerda, H. Espinoza-Gómez, G. Alonso-Núñez, I.A. Rivero, Y. Gochi-Ponce, L.Z. Flores-López, A green synthesis of copper nanoparticles using native cyclodextrins as stabilizing agents, J. Saudi Chem. Soc. 21 (2017) 341–348, https://doi.org/10.1016/j.jscs.2016.10.005.
[29] L. Gritsch, C. Lovell, W.H. Goldmann, A.R. Boccaccini, Fabrication and characterization of copper(II)-chitosan complexes as antibiotic-free antibacterial biomaterial, Carbohydr. Polym. 179 (2018) 370–378, https://doi.org/10.1016/j.carbpol.2017.09.095.
[30] T. Jayaramudu, G.M. Raghavendra, K. Varaprasad, R. Sadiku, K. Ramam, K.M. Raju, Iota-Carrageenan-based biodegradable Ag^0nanocomposite hydrogels for the inactivation of bacteria, Carbohydr. Polym. 95 (2013) 188–194, https://doi.org/10.1016/j.carbpol.2013.02.075.
[31] T. Jayaramudu, K. Varaprasad, G.M. Raghavendra, E.R.R. Sadiku, K. Mohana Raju, J. Amalraj, Green synthesis of tea Ag nanocomposite hydrogels via mint leaf extraction for effective antibacterial activity, J. Biomater. Sci. Polym. Ed. 28 (2017) 1588–1602, https://doi.org/10.1080/09205063.2017.1338501.
[32] T. Jayaramudu, K. Varaprasad, H.C. Kim, A. Kafy, J.W. Kim, J. Kim, Calcinated tea and cellulose composite films and its dielectric and lead adsorption properties, Carbohydr. Polym. 171 (2017) 183–192, https://doi.org/10.1016/j.carbpol.2017.04.077.
[33] O. Ejeromedoghene, S. Adewuyi, S.A. Amolegbe, C.A. Akinremi, B.A. Moronkola, T. Salaudeen, Electrovalent chitosan functionalized methyl-orange/metal nanocomposites as chemosensors for toxic aqueous anions, Nano-Struct. Nano-Objects 16 (2018) 174–179, https://doi.org/10.1016/j.nanoso.2018.06.004.
[34] E. Tabesh, H.R. Salimijazi, M. Kharaziha, M. Mahmoudi, M. Hejazi, Development of an in-situ chitosan-copper nanoparticle coating by electrophoretic deposition, Surf. Coatings Technol. 364 (2019) 239–247, https://doi.org/10.1016/j.surfcoat.2019.02.040.
[35] C.-H. Du, C.-J. Wu, L.-G. Wu, Effects of pluronic F127 on the polymorphism and thermoresponsive properties of PVDF blend membranes via immersion precipitation process, J. Appl. Polym. Sci. 124 (2012) E330–E337, https://doi.org/10.1002/app.35257.
[36] J. Qi, W. Zhao, B. Wang, S. Ding, L.S. Daintree, D.M. Ledger, W. Wu, X. Yin, H. Jiansheng, Itraconazole solid dispersion prepared by a supercritical fluid technique: preparation, in vitro characterization, and bioavailability in beagle dogs [Corrigendum], Drug Des. Devel. Ther. 4387 (2015) https://doi.org/10.2147/DDDT.S91738.
[37] W.H. Eisa, A.M. Abdelgawad, O.J. Rojas, Solid-state synthesis of metal nanoparticles supported on cellulose nanocrystals and their catalytic activity, ACS Sustain. Chem. Eng. 6 (2018) 3974–3983, https://doi.org/10.1021/acssuschemeng.7b04333.
[38] K. Li, S. Jin, H. Chen, J. Li, Bioinspired interface engineering of gelatin/cellulose nanofibrils nanocomposites with high mechanical performance and antibacterial properties for active packaging, Compos. Part B Eng. 171 (2019) 222–234, https://doi.org/10.1016/j.compositesb.2019.04.043.
[39] D.G. Deryabin, E.S. Aleshina, A.S. Vasilchenko, T.D. Deryabina, L.V. Efremova, I.F. Karimov, L.B. Korolevskaya, Investigation of copper nanoparticles antibacterial mechanisms tested by luminescent Escherichia coli strains, Nanotechnol. Russ. 8 (2013) 402–408, https://doi.org/10.1134/S1995078013030063.
[40] J. Jung, G.M. Raghavendra, D. Kim, J. Seo, One-step synthesis of starch-silver nanoparticle solution and its application to antibacterial paper coating, Int. J. Biol. Macromol. 107 (2018) 2285–2290, https://doi.org/10.1016/j.ijbiomac.2017.10.108.
[41] T. Jayaramudu, G.M. Raghavendra, K. Varaprasad, R. Sadiku, K.M. Raju, Development of novel biodegradable Au nanocomposite hydrogels based on wheat: for inactivation of bacteria, Carbohydr. Polym. 92 (2013) 2193–2200, https://doi.org/10.1016/j.carbpol.2012.12.006.